TAO, Supplementary Issue, 145-164, March 1999

Ka Band Propagation Experiments of Experimental Communication Payload (ECP) on ROCSAT-1 – Preliminary Results

Shun-Peng Shih[1] and Yen-Hsyang Chu[1]

(Manuscript received 9 November 1998, in final form 8 January 1999)

ABSTRACT

It is recognized that rain attenuation is the primary factor in the degradation of Earth-satellite communication at the Ka band frequency. The beacon signal of the ROCSAT-1 is set at 19.5 GHz for downlink and 28.5 GHz for uplink. ROCSAT-1 is the low earth orbit (LEO) satellite with a circular orbit at the altitude of 600 km and 35° inclination angle and scheduled to be launched at the beginning of 1999. Given the extremely high frequency of the beacon, impairment of ROCSAT-1 communications due to rain attenuation should be seriously considered. In this paper, the ground-based instruments for the Ka band propagation experiments of ROCSAT-1, including Chung-Li VHF radar, 19.5 GHz radiometer, optical rain gauge, automatic weather station, and disdrometer, are introduced. The spatial distribution of the long-term statistics of rainfall rate is analyzed in this paper on the basis of 8 years (1988-1995) rainfall rate data at one-minute time resolution, recorded by more than 70 tipping bucket rain gauges distributed over Taiwan island. It shows a pronounced latitudinal variation in the percentage of time that the rainfall rate exceeds a specified level, indicating that more severe rain attenuation will be encountered in the southern part than that in the northern part of Taiwan. In addition, the sky noise temperature at the frequency of 19.5 GHz is measured by using a radiometer, both in the conditions of clear-air and precipitation. The observed sky noise temperature in the case of clear-air at the elevation angles of 90°, 60°, 30°, and 15° are respectively 50K, 80K, 100K, and 130K, corresponding to the attenuations of 0.7dB, 0.78dB, 1.2dB, and 2.7dB. Data analysis indicates that the observed clear-air sky noise temperature increasing exponentially with the decrease of the zenith angle is in perfect agreement with our theoretical prediction. The sky noise temperature in the case of precipitation is also investigated. A comparison between observed precipitation sky noise temperature and surface rainfall rate shows that a salient time shift in the two is seen, implying that great caution should be taken in

[1]Institute of Space Science, National Central University, Chung-Li, Taiwan, ROC

establishing an empirical relationship between precipitation sky noise temperature and surface rainfall rate.

(Key words: Ka band, Propagation experiment, ROCSAT-1, Rain attenuation)

1. INTRODUCTION

According to the national fifteen-year space program implemented by the National Space Program Office (NSPO), a low-earth orbit (LEO) experimental satellite, ROCSAT-1, is scheduled to be launched at the end of January 1999. The satellite will orbit the Earth at an altitude of 600 km with an inclination of 35° and an orbital period of 97 minutes. The frequency of occurrence for the beam downlink telemetry to signal collected data to local receiving stations will be about 6 times per day. There are three payloads mounted on the ROCSAT-1. First is the Ocean Color Imager (OCI) for remote sensing of the pigment distribution in the low-latitude oceans for the oceanography research. Second is the Ionospheric Plasma and Electrodynamics Instrument (IPEI) used to take the measurements of ionospheric parameters, such as plasma density, plasma temperature, electric field strength, plasma drift velocity, and so on. Third is the Experimental Communication Payload (ECP) designed for the communication experiments, which include the high data rate (> 6.6 Mbps) communication experiment, low data rate (< 256 Kbps) communication experiment, and the Ka band propagation experiment. The transmitted frequencies for the uplink communication channel of the ECP experiment are within the range of 28 ~ 28.5 GHz, while the down link frequencies of the beacon and communication channels are respectively 19.5 and 18.2 ~ 18.7 GHz. It is generally recognized that the electromagnetic waves in the Ka band are susceptible to weather-related precipitation, impairing the quality of the Earth-satellite communication (Hogg and Chu, 1975). It is well known that the effects of rain attenuation on Ka band propagation occur through the mechanisms of absorption of water vapor and oxygen molecules and scattering of precipitation particles. Furthermore, the depolarization effect due to the non-spherical shape of rain drops is another factor influencing the attenuation of Ka band signal. In addition, the scintillation of the signal induced by the diffraction of atmospheric refractivity irregularities and the abnormal refraction caused by the waves propagating through the highly stratified atmospheric structures also play crucial roles in the degradation of the earth-satellite communication link.

Because an orbiting LEO satellite continuously changes its angular position (or range with respect to a ground receiving station) during the course of its pass, the propagation effects on the communication link of a LEO satellite, as mentioned above, will vary with the elevation angle of the satellite. For example, the free-space path loss, a vital factor in the performance of the LEO satellite, will be different during the satellite flight. The magnitudes of the rain attenuation and gaseous absorption will be also changed with the location of satellite in its path. In this regard, the quality of LEO satellite communications will be impaired if the margin of the communication link is not large enough to overcome the angular change in the signal attenuation. Therefore, in order to maintain the high quality of the communication link of a LEO satellite, the propagation effects of a LEO satellite should be investigated thoroughly.

The elevation angle variation in the Ka band transmission loss for a LEO satellite has been studied by Ippolito and Russell (1993). They show that, as the elevation angle varies, so does the length of the radio transmission path and the free space loss incurred on the path. After analyzing the annualized outage probability at Ka band derived from rain statistics for a single pass of a LEO satellite, Ippolito and Russell (1993) conclude that the link reliability varies drastically over the course of a LEO satellite pass and the outage probability averaged over the entire pass should be considered as an essential design criterion.

In order to understand the characteristics of the propagation channel at Ka band over the Taiwan area for the purpose of designing an optimal earth-satellite communication link, the atmospheric effects influencing the quality of satellite communication mentioned above should be investigated thoroughly. The objectives of the Ka band propagation experiment of ROCSAT-1 are (1) to study the characteristics of rain attenuation at the frequency of Ka band, (2) to understand the behavior of scintillation caused by atmospheric refractivity fluctuations and rain over Taiwan area, (3) to investigate the depolarization effect on Ka band signal due to non-spherical rain drops, (4) to carry out the site diversity experiment to measure the diversity gain for the compensation of rain attenuation effect, (5) to conduct the multi-path and low-elevation propagation using the beacon signal of the ROCSAT-1 satellite. Moreover, the establishment of the data base of the propagation experiment through the persistent collection of the propagation experiment-related data, including high quality surface rainfall rate, background sky noise temperature, weather information (wind speed, wind direction, humidity, temperature, pressure, and so on), and radar data, is also an important task for the design of an optimal satellite communication link.

In this paper, the long-term statistics of the rainfall rate at the time resolution of one minute from 1988 - 1995 observed by using more than 70 ground-based tipping bucket rain gauges over Taiwan island are analyzed and investigated. The results indicate a latitudinal variation in the percentage of the times that the rainfall rate exceeds a certain level; it is larger in the southern part of Taiwan and smaller in the northern part of Taiwan. This feature implies that the rain attenuation effect on Ka band propagation is more severe in the southern part than in the northern part of the island. Furthermore, in order to estimate the possible impairment of the LEO satellite communication link due to rain attenuation, the variation in the rain attenuation at the Ka band with the zenith angle is examined below. In addition, this article compares the rainfall rate measured by a high performance optical rain gauge and the sky noise temperature observed by a radiometer centered at 19.5 GHz.

2. INSTRUMENTS EMPLOYED FOR Ka BAND PROPAGATION EXPERIMENT

2.1 Chung-Li VHF Radar

Rain height is a crucial parameter in estimating the rain attenuation of a satellite communication signal. Conventionally, rain height is scaled from the temperature profile observed by a rawinsonde, in which the height of 0°C isotherm is thought to be the thickness of rain. However, the rain height thus obtained is not necessarily the one exactly above the rawinsonde station. This is because the path of the balloon subjected to the drift of the horizontal wind is

slanted, not vertical. Moreover, the balloon is launched every 12 hours, either at 00 UT or 12 UT. Therefore, it is inefficient and inaccurate to use the 0°C isotherm height obtained from rawinsonde to find the rain height for the purpose of estimating rain attenuation in the propagation experiment. However, with the capability of simultaneously observing precipitation particles and refractive index fluctuations, it is convenient to estimate the actual rain height from the height of the bright band in the profile of precipitation echoes measured by a VHF radar (Chu et al., 1991; Chu and Lin, 1994; Chu and Song, 1998). The Chung-Li VHF radar is located on the campus of National Central University in Taiwan, Republic of China. This radar consists of three independent but identical modules; each of the modules contains its own transmitter, receiver, antenna array, signal preprocessor, and other essential system units. The operational frequency of Chung-Li VHF radar is 52 MHz (corresponding to 5.77 m wavelength) and the peak transmitted power is 180 kW (3X60). The maximum duty cycle is 2%, and the pulse width can be set arbitrarily from 1 μs to 999 μs. Two phase coding schemes are implemented on Chung-Li VHF radar for different purposes of the experiment. One is the complementary code with adjustable code length of 2, 4, 8, and 16 elements. The other one is the Barker code with adjustable code length of 7, 9, 11and 13 elements. The antenna array of Chung-Li VHF radar used for tropo-, strato-, and mesospheric (MST) experiment consists of three square antenna modules with 64 Yagi antenna elements (8X8) each. The whole antenna array is arranged as a triangle with equal lateral sides with respective lengths of 45, 45, and 40 m. Besides its vertical direction, the boresight of the antenna main beam for each module can also be pointed obliquely toward the north, west, south, or east with a fixed 17° zenith angle. Note that the azimuthal direction toward which the antenna beam is steered is not the cardinal geographical north, west, south, or east, but has a counterclockwise 22.3° azimuthal angular difference from the respective cardinal geographical direction. The total physical antenna area is 4800 m^2 (3X40X40). The main antenna beam for each module has a half-power-beam width of 7.4°. The detailed characteristics of the Chung-Li VHF radar are summarized in Table 1. For more information on the characteristics of the Chung-Li VHF radar, see Rottger et al. (1990).

2.2 19.5 GHz Radiometer

Radiometry is the measurement of electromagnetic radiation from an object with a certain temperature. A microwave radiometer is a highly sensitive receiver capable of measuring low levels of microwave radiation. When an object, such as a hydrometeor particle, water vapor, an oxygen molecule, or atmospheric turbulence, is observed by a microwave radiometer, the radiation received by the antenna is partly due to self-emission by the object and partly due to radiation originating from the surroundings. Through proper choice of the radar parameters (wavelength, polarization, and viewing angle), sometimes it is possible to establish useful relations between the magnitude of the energy and the phase received by the radiometer and specific terrestrial or atmospheric parameters of interest. The central frequency of the radiometer employed for the Ka band propagation experiment is 19.5 GHz. This radiometer is a single linearly polarized (orientation of the feed horn determines vertical or horizontal polarization), superheterodyne, Dicke-switched instrument with the following characteristics: cen-

Table 1. Characteristics of Chung-Li VHF Radar.

Location	Chung-Li, Taiwan, Republic of China
Coordinate	Geographic latitude: 24.9° N ; longitude: 121° E ; Geomagnetic latitude: 13.3° N ; longitude: 189.3° ; Dip angle: 35° N
Frequency	52 MHz (5.77 m radar wavelength)
Peak Transmitted Power	0.18 MW
Pulse Length	1 ~ 999 μs
Maximum Duty Cycle	2%
Maximum Nyquest Frequency	~ 160 Hz
Antenna Array	
Type	3 rectangular arrays with 32 Yagi elements (4X8) each
Configuration	arranged as a triangle with the side length of 40m, 80m, and 92m, and apex toward the southwest by 17°
HPBW	7.4° x 15°for each module (elliptic beam)
Steerability	northward with a fixed zenith angle of 41° (normal to geomagnetic field line at 250 km)
Total geometric area	3X800 m^2
Receiver Bandwidth	Matched filter: 1MHz, 0.5MHz, 0.25 MHz, 125KHz, 62.5 KHz and 23 KHz
Phase Code	Complementary Code with 2, 4, 8, 16 elements Barker Code with 7, 9, 11, 13 elements

ter frequency, 19.5 GHz; IF bandwidth, 500 MHz (both signal and image bands are received, i.e., spectral coverage is from 19 to 20 GHz with a 10 MHz notch at 19.5 GHz); sensitivity, approximately 0.5 K for an integration time of 1 sec; and polarization, single linear of either horizontal or vertical. The horizontal or vertical voltage signal from the radiometer is fed into the low pass filter/amplifier which determines the integration time of the radiometer. The low pass filter used for the measurements reported here has a various cutoff frequency for the integration time between 4 and 1024 mini-seconds. The horizontal or vertical signal from the low pass filter is sent to a printer/recorder for viewing the data in real time and to a data collection board connected to the bus of the host IBM personal computer that controls the data acquisition. The data collection board digitizes the radiometer output with 12 bit precision. The beam width of the 19.5 GHz antenna is approximately 6 degrees and the data may be sampled every 3 degree in both azimuth and elevation so that the information is Nyquist sampled. The position in azimuth and elevation shall be recorded each time the radiometer signals are

sampled. The low pass filters for the radiometer are set to an integration time in the range of 4 to 1024 ms. The 19.5 GHz radiometer has a Dicke reference load and an avalanche noise diode that serves as an internal calibration source. The equivalent temperature of the noise diode, referred to as DTCAL, is determined in the laboratory by viewing external loads at room temperature and at liquid nitrogen temperature. These laboratory measurements shall be performed both before and after field deployments. During field measurements the Dicke reference and the avalanche noise diode shall be viewed before and after each run. The detailed characteristics of 19.5 GHz Radiometer are summarized in Table 2.

2.3 Optical Rain Gauge

The rain gauge collecting the surface precipitation data is an essential tool in performing the rain attenuation experiment. Conventionally, the rain rate data collected by the tipping

Table 2. Characteristics of Microwave Radiometer.

Central Frequency/Polarization	19.5 GHz/Single Linear
Input Bandwidth	1 GHz
IF Bandwidth	500 MHz
Antenna	Conical Feedhorn
Half Power Beam Width of Horn Antenna	6°
Noise Figure	
Mixer-Preamplifier	4.0 dB
Isolator	0.3 dB
Filter	0.2 dB
Latching Circulator	0.3 dB
Waveguide	0.2 dB
In Total	5.0 dB
Integration Time	4 ~ 1024 msec
Input Range	0 ~ 313 K
Sensitivity	0.5 ~ 1 K
Accuracy	1 ~ 2 K
Switch Rate	2,2 KHz
Dynamic Range	0 ~ 350 K
Receiver Type	Superheterodyne, Double-Sideband, Noise-Injection Dickie Type
Size	30"L x 18"W x 12"H
Weight	25 lb
Power Supply	120 V, 60 Hz, 5 Amp Max.

bucket rain gauge is analyzed to obtain the long-term statistics of rain rate. However, the data thus observed are susceptible to the effects of wind loss and splash in/out. In order to avoid these effects on the collected rain rate quality, the use of another type of rain gauge is necessary. The rain gauges employed for the propagation experiment are the ScTI's (Scientific Technology, Inc.) Series optical rain gauges (ORG), which can provide accurate measurement of the precipitation in all weather conditions with high temporal resolution. This kind of rain gauge, designed for rugged, unattended operation, has been proven in adverse environments, including land sites and ocean deployed data buoys and ships. The sensors offer easy field calibration capability and a simplified interface to data loggers and data acquisition systems. Precipitation is measured by detecting the optical irregularities induced by drops falling through an infrared optical beam. These irregularities causing the scintillation of signals have characteristic patterns which are detected by the sensor and converted to precipitation rate. ScTI Optical Rain Gauges are not affected by many of the environmental factors which cause significant errors with traditional rain gauges. Traditional mechanical gauges such as tipping bucket, siphon, and weighing type gauges will suffer from wetting losses, evaporation losses, wind losses, rain incident angle sensitivity, splash in/out, effects from debris and insects, effects from dust and silt accumulation, and poor performance for solid precipitation. However, none of these effects cause errors in the measurements of precipitation made with optical rain gauge. The detailed characteristics of optical rain gauge Model ORG-815 are summarized in Table 3.

2.4 Disdrometer

The drop-size distribution of the hydrometeor in the path of the Earth-satellite communication link is a vitally important parameter in the investigation of rain attenuation. Although the measurement of drop-size distribution aloft by using a VHF radar has been reported (Wakasugi et al., 1986), the drop-size distribution near the ground can not be obtained by VHF radar. The only one way to measure the surface drop-size distribution is to use the disdrometer. Besides distribution of the hydrometeor, many precipitation-related parameters, such as rain fall rate and the shape of hydrometeor, can also be obtained through disdrometer measurements. Various types of distrometers measure some of these other interesting parameters and in many cases some others have to be set to predefined values, taken from the literature. In this context the idea for a new development has come up: a new instrument that would measure all the relevant parameters. The disdrometer employed for the propagation experiment is the 2D-Video-Distrometer. The 2D-Video-Distrometer is designed to meet the needs generally of our experiment. The measurements of this disdrometer reveal classification of precipitation at the measurement site as well as full particulars on single hydrometeors. Of each raindrop, snowflake, hailstone reaching the measuring area, the front view, the side view and the velocity can be measured and recorded using this instrument. The resolution of the digitizing grid is on the order of 0.25 mm. For a reliable classification of precipitation event distributions of size and velocity of particles as well as of oblateness of drops are generated in real time. The instrument operates fully automatically, 24 hours per day. The system components of the 2D-Video-Distrometer consist of the three main units described below: the Sensor Unit (SU), Outdoor

Table 3. Characteristics of Optical Rain Gauge (Model ORG-815).

Measure Range	0.1 ~ 500 mm/hr
Accuracy	5% from 1 to 500 mm/hr
Resolution	0.001 mm
Rain Accumulation	0.001 ~ 999.9 mm
Time Constant	10 seconds
Data Update Rate	Once per minute – typical Every 5 seconds - available
Supply Voltage	11 – 16 VDC
Current Drain	500 - 800 mAmp
Signal Output	RS-232
Operational Environment	
Temperature	-40 to 50°C
Relative Humidity	0 – 100%
Size	30"L x 18"W x 12"H
Weight	25 lb
Cable Length	15 meters

Electronics Unit (OEU), and Indoor User Terminal Unit (IUT). OEU is located not more than 5 meters distant from the SU. The OEU controls the video cameras, acquires the raw data and performs preprocessing and data compression. The Indoor User Terminal (IUT) stores the data and gives a graphic display. The distance from IUT to OEU may be up to 300 meters. A main cable and a 50 Ohms coaxial cable for data are connected to the OEU. Two line scan cameras are directed towards the openings of the illumination devices. The optical system is designed in such a way that (seen through the camera lens) the slit of the illumination device appears as an evenly illuminated background of extreme brightness. To the cameras, any particle falling through the beam of light will appear as a dark silhouette against this bright background. Note that in the actual instrument each of the two optical paths contains two mirrors that are used to "bend" the beam. These are left out here to simplify the drawing. The virtual measuring area is located a few centimeters beneath the rims of the collecting funnel, thus avoiding the unwanted effect of splashing from these rims into the virtual measuring area. The mechanical structure consists of two parts. The inner part carrying all optical components is mounted on just four rubber shock absorbers. This guarantees that the adjustment of the optical parts is not impaired by any mechanical influences like heavy wind, opening of the housing and so forth. The outer part carries the inner one and shields it against water. The instrument is easy to open, all components are easily accessible. Calibration and maintenance procedures are easy to perform and quickly done. To check the calibration, a number of precision spheres of various diameters have to be dropped into the receiver. Results are given on the IUT. Nor-

mally there is no need for readjustments. On-line, the following displays are available: rainrate vs. time, dropsize distribution, vertical velocity vs. equivolumetric diameter, horizontal velocity, oblateness vs. diameter. These five displays and the single hydrometeor display may be selected for full screen representation with additional information and further menu choices. A top view of the measuring area is drawn. It may be set to a mode indicating the distribution of hydrometeors over the measuring area by means of a colour code. Due to the measurement by line scan cameras, horizontal velocities introduce distortions, as lines are shifted against each other. The horizontal velocity of raindrops is approximately determined and on that basis a correction is applied. Determination of equivolumetric diameter, volume, vertical velocity and of oblateness defined as the ratio width/height is independent of horizontal velocity. It should be noted that the display allows the user the choice of various parameters and display filter options. The criterion for integration intervals size distributions can be chosen to be either a number of hydrometers or a time interval or an amount of rainfall. Also the integration interval for the rainrate may be freely chosen. The rain total is also displayed. These choices allow detailed studies of hydrometeors as well a reliable system performance analysis. The IUT operation program offers all these display options to the user while storing data to the disk. An off line version of the display program allowing studies of recorded data offers the same display features as the online version. A detailed description of the characteristics of the 2D-Video-Distrometer is summarized in Table 4.

3. STATISTICS OF RAINFALL RATE OVER THE TAIWAN AREA

The data employed for the long-term statistical analysis are the rainfall rates at one-minute time resolution collected by more than 70 tipping bucket rain gauges distributed over Taiwan

Table 4. Characteristics of 2D-Video-Disdrometer.

Measure Range	approximately 100 x 100 mm^2
Vertical Velocity Accuracy	better than 5 %
Resolution (horizontal)	better than 0.22 mm
Resolution (vertical)	better than 0.3 mm for velocity < 10 m/s
Integration Time	15 sec to 12 hours
Supply Voltage	110/220/240/V, 50/60 Hz
Power Consumption	500 W
Operating Temperature	-10 to 40°C
Survival Temperature	-20 to 60°C
Weight	130 Kg
Height	110 cm
Width	60 cm
Length	150 cm

island from 1988 to 1995. From the cumulative distribution of the rainfall rate, the percentage of time in a year the rainfall rate is exceeded can be obtained. Figure 1a shows an example of the cumulative distribution of rainfall rate recorded by the tipping bucket rain gauge located at Chung-Li station (24.9°N, 121.5°E). It indicates that the percentages of time rainfall rate exceeds 20, 50, 80, and 100 mm/hr are respectively about 0.12% (10.51 hr), 0.033% (2.88 hr), 0.006% (31.5 min), and 0.0038% (20 min). In order to examine the quality of the statistics of rainfall rate recorded by tipping bucket rain gauge, the rainfall rate observed by another kind of rain gauge, i.e., an optical rain gauge, is employed for comparison. Figure 1b presents the cumulative distribution of rainfall rate measured by optical rain gauge from November 1, 1996 to October 31, 1997. Comparing Figure 1a and 1b reveals that the general behavior of the statistics obtained by tipping bucket and optical rain gauge is very similar, irrespective of the slight difference in the curve shape and the magnitude of the percentage between them. This result implies that the rainfall rate data collected by tipping bucket rain gauge are reliable and the statistics thus obtained are acceptable.

The magnitude of rain attenuation A for terrestrial and earth-satellite links can be calcu-

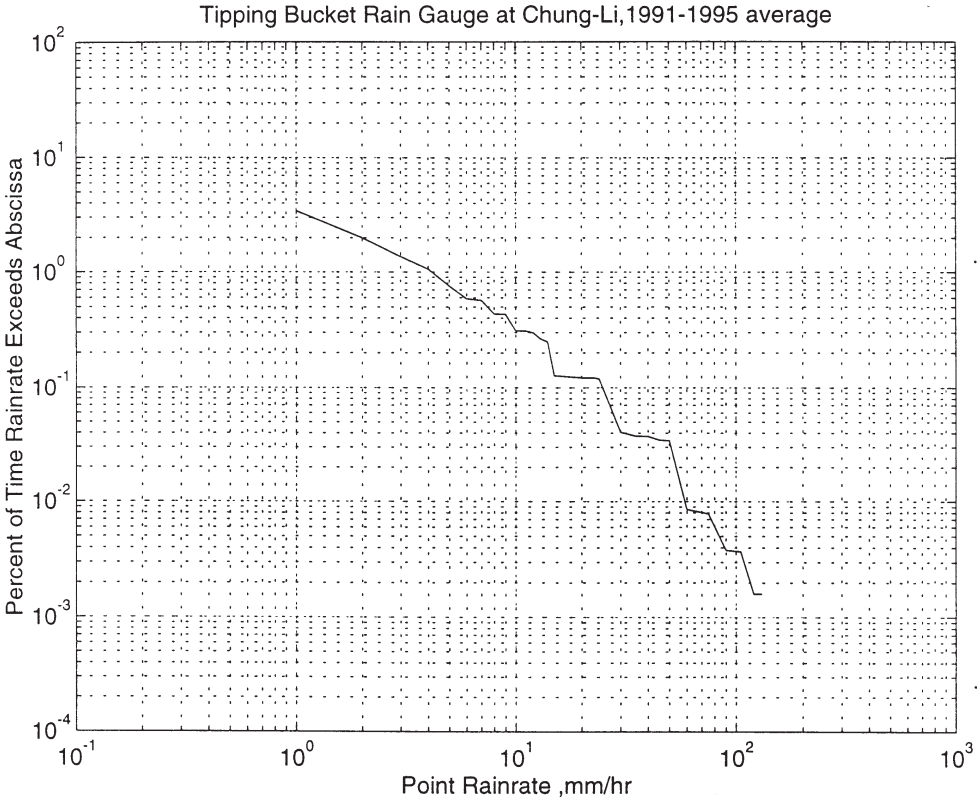

Fig. 1a. An example of the cumulative distribution of rainfall rate recorded by the tipping bucket rain gauge located at Chung-Li station (24.9°N, 121.5°E) from 1988 to 1995.

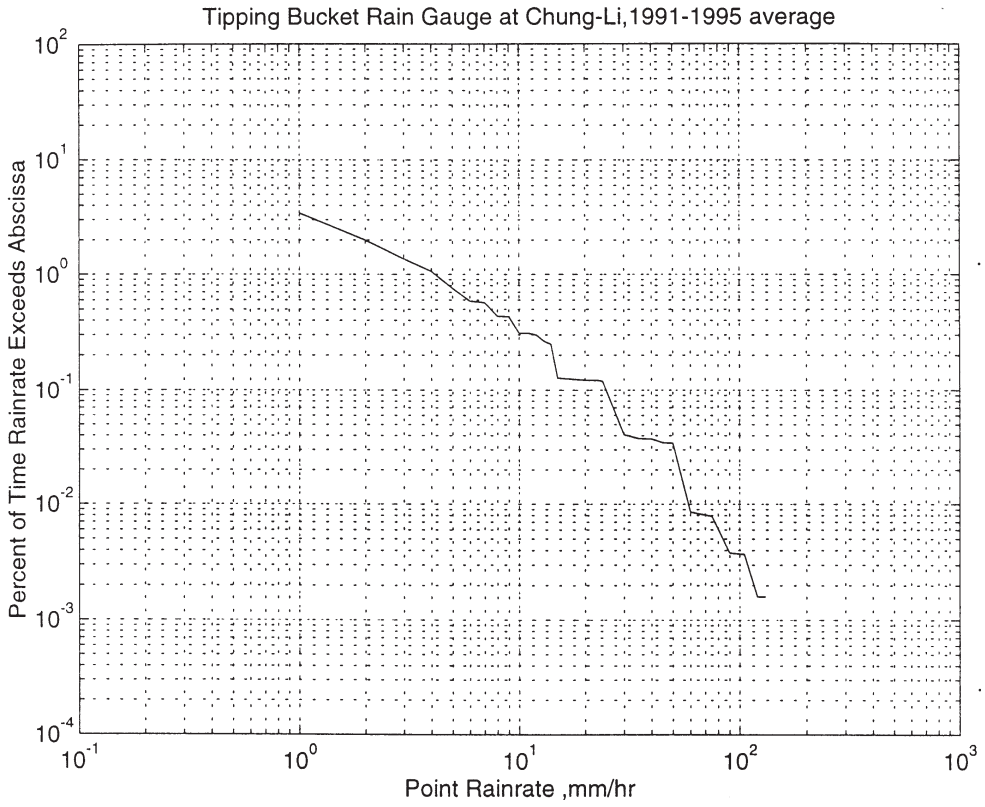

Fig. 1b. Cumulative distribution of rainfall rate measured by optical rain gauge located at Chung-Li from November 1, 1996 to October 31, 1997.

lated from the point rainfall rate R_p in accordance with the following equation

$$A = L(R_p)\gamma(R_p) \tag{1}$$

where $\gamma(R_p)$ is the specific rain attenuation in the unit of dB/km and L(Rp) is the effective path length. The relation between $\gamma(R_p)$ and R_p has been shown empirically and theoretically that it can be expressed in the form of (Olsen et al., 1978)

$$\gamma(Rp) = aR^b \tag{2}$$

where a and b are the functions of radio wave frequency, drop-size distribution, and rain temperature. A number of investigators have examined the power-law relation as shown in equation (2) and obtained the empirical values of a and b (Harrold, 1967; Semplak and Turrin, 1969). In the case of Laws and Parsons drop-size distribution and 20°C rain temperature, the corresponding values of a and b for frequencies 20 and 30 GHz are 0.0699, 1.10 and 0.170 and 1.075, respectively (Crane, 1980). An empirical relation connecting effective path length $L(R_p)$

with the elevation angle of satellite θ and the point rainfall rate Rp has been obtained by Rogers (1980) as shown below

$$L(Rp, \theta) = [0.00741Rp^{0.766} + (0.232 - 0.00018Rp)\sin\theta]^{-1} \quad (3)$$

The total amount of rain attenuation A can thus be calculated in accordance with equations (1) ~ (3). It is noteworthy that equation (3) is obtained through long-term statistical analysis and is inappropriate for estimating the instantaneous rain attenuation of the satellite signal. On the basis of the long-term statistics of rainfall rate recorded at Chung-Li, Figure 2 presents the variations of the rain attenuation with the elevation angle of satellite for the specific point rainrate 5.5, 32.5, and 88 mm/hr, which correspond respectively to the percentage of time 1.0%, 0.1%, and 0.01% in a year rainfall rates are exceeded. As shown, a considerable variation in the rain attenuation with the elevation angle is seen, changing from 17 dB at 70° to 39 dB at 10° for the rainfall rate of 32.5 mm/r and from 31 dB at 70° to 58 dB at 10° for 88 mm/hr. In view of the large variation in rain attenuation with elevation angle, the propagation margin should be large enough to achieve high link reliability in designing the communication link for a LEO satellite.

Taiwan is an island with rough terrain; two-thirds of the island is covered by the high

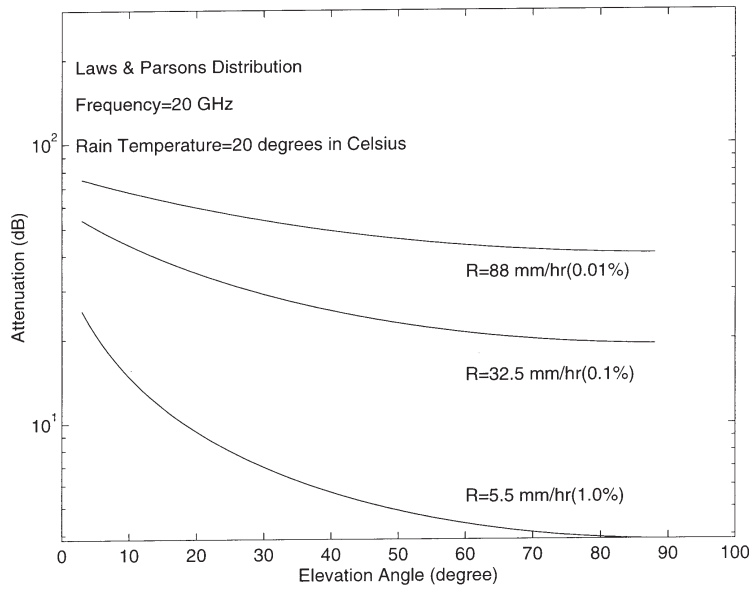

Fig. 2. Variations in the estimated rain attenuation with the elevation angle of satellite for the specific point rainrate 5.5, 32.5, and 88 mm/hr, which correspond respectively to the percentage of time 1.0%, 0.1%, and 0.01% in a year rainfall rates are exceeded. The long-term statistics of the 8 years rainfall rate used for calculation is taken from the data collected at Chung-Li.

mountains and small hills. The altitude difference between the highest and lowest points in the island is about 3900 m. Because the orographic effect combined with the wind pattern associated with the monsoons greatly governs the behavior of the rainfall, it is expected that the statistical characteristics of the rain over Taiwan area will differ with location. Employing the rainfall rate data recorded by more than 70 tipping bucket rain gauges distributed over Taiwan island, the spatial distribution of the rainfall rate can be obtained. Figure 3a, 3b and 3c present

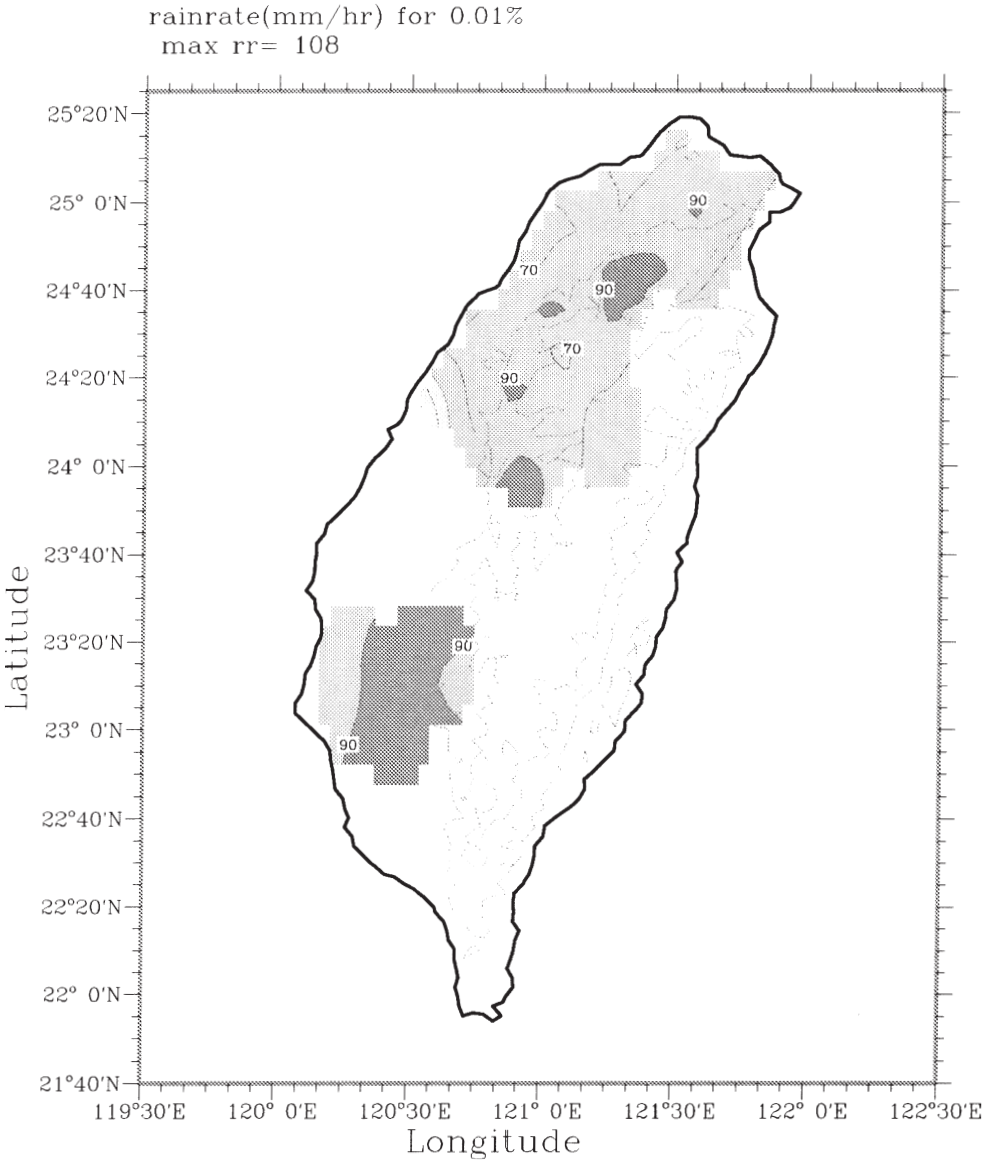

Fig. 3a. Spatial distributions of the specific rainfall rate corresponding to the percentages of the time of the year 0.01% rainfall rate exceeds.

the contour plots of the spatial distributions of the specific rainfall rate for the percentages of the time of the year 0.01%, 0.1%, and 1.0%, respectively. The rainfall rates employed for the Figure 3a, 3b, and 3c are taken from the data collected by the network of tipping bucket rain gauges deployed by the Central Weather Bureau. The rainfall rate recorded by several rain gauges sites in the network in the central and southern parts of Taiwan are found to be erroneous and not suitable for the analysis. This is the reason why there are data blanks in the central

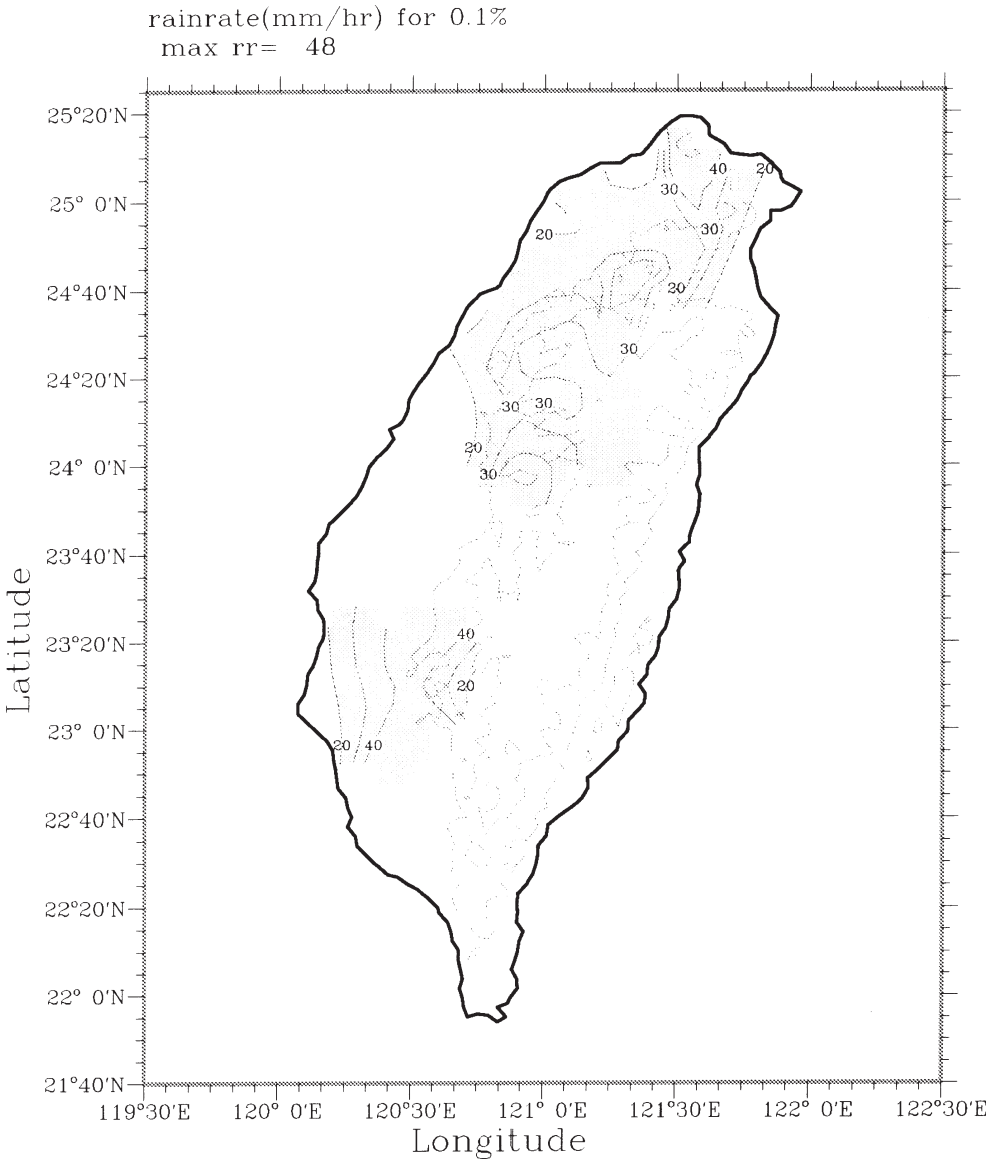

Fig. 3b. Same as figure 3a, but for the percentage of time 0.1% rainfall rate exceeds.

and southern part of Taiwan. Comparison of figures 3a, 3b and 3c indicates that for the case of intense rainfall rates (i.e., 0.01% percentage of time) the rainfall rate in the southern part of Taiwan is greater than that in the northern part of Taiwan, while for the light rain cases (i.e., 10.% percentage of time) the rainfall rate in northern part of Taiwan is larger than that in southern part of Taiwan. As mentioned previously, this is because in the Taiwan area the wind pattern in the winter season is controlled by the north-east wind, many rains are produced in

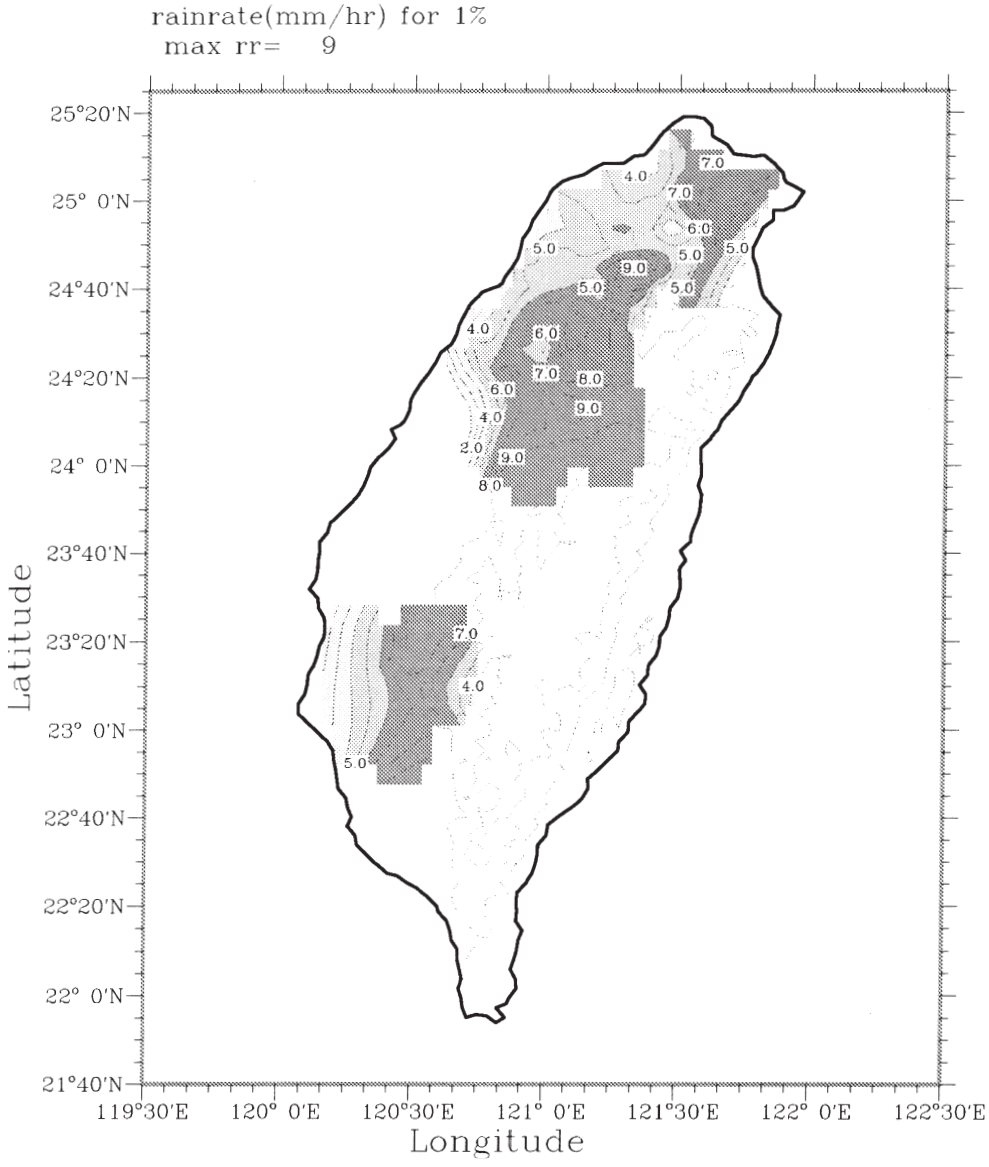

Fig. 3c. Same as figure 3a, but for the percentage of time 1.0% rainfall rate exceeds.

the north-east part of Taiwan due to orographic effect. Similarly, the south-west wind prevails in the summertime and generates heavy rain in the south-west region of Taiwan island. Because the rain attenuation is directly related to the intensity of the rain, the feature of the latitudinal variation of the rainfall rate over Taiwan area reveals that the reliability of earth-satellite communication link operated at Ka band in the northern part of Taiwan will be much higher than that in the southern part of Taiwan.

4. RADIOMETER MEASUREMENTS

The radiometer is an important instrument in the investigation of the propagation effects on the microwave communication channel, especially for the rain attenuation and gaseous (water vapor and oxygen molecule) absorption effects. A well-calibrated radiometer at the central frequency of 19.5 GHz was set up on the campus of National Central University at

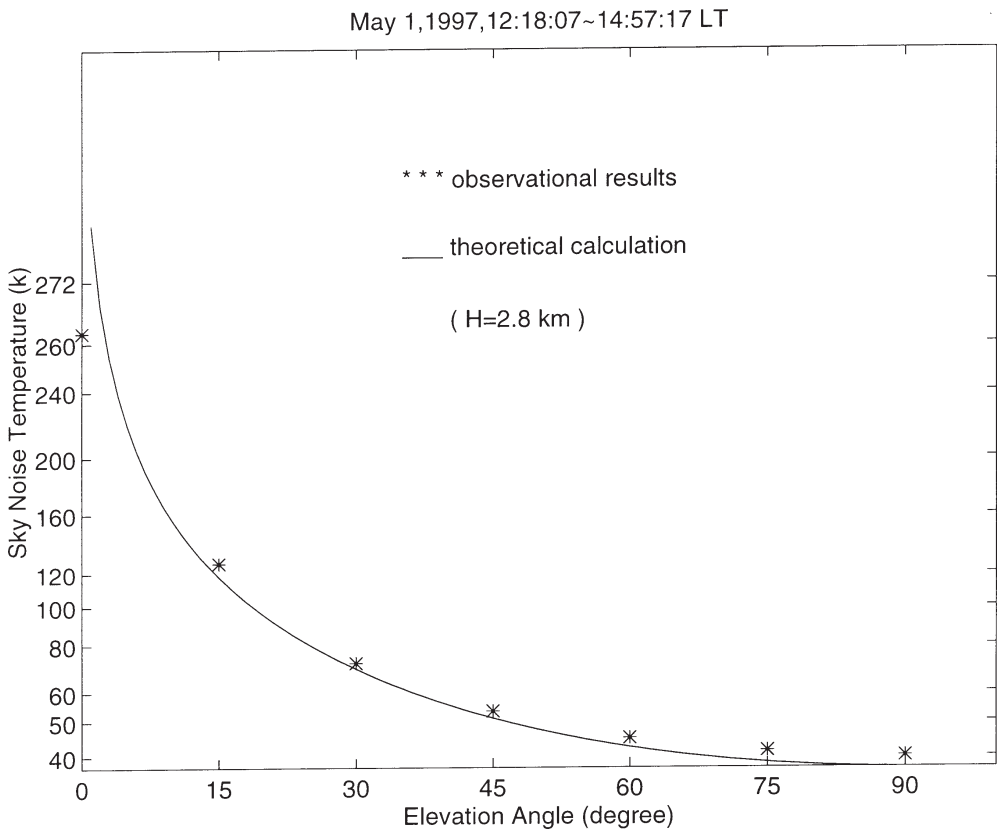

Fig. 4. Comparison of the observed clear-air sky noise temperature with the theoretical calculation, where the scale heights of water vapor and oxygen molecule are adopted as 2.8 km and 8.6 km, respectively.

Chung-Li in the spring of 1997 to measure the background sky noise temperature and the radiation from the precipitation particles. The characteristics of the radiometer are listed in Table 3. Figure 4 presents the variation of the measured clear-air sky noise temperature with the elevation angle of the horn antenna of the radiometer, in which asterisk points are the observed values and the solid curve is the theoretical result. To calculate the theoretical clear-air sky noise temperature for slant path, we follow the method suggested by Ippolito (1986) by assuming the height variation of the concentrations of the water vapor and oxygen molecules to be exponential and the scale height of water vapor and oxygen molecules to be 2.8 km and 8.6 km, respectively. As indicated in figure 4, the theoretical calculation is in perfect agreement with the observations and the observed sky noise temperatures at the elevation angles 90°, 75°, 60°, 45°, 30°, and 15° are respectively 40 K, 42 K, 46 K, 53 K, 72 K, and 128 K.

The sky noise temperature generated from the rain drops is also measured in this study. The mathematical relation converting the observed sky noise temperature T_b radiated by the precipitation particles with the temperature T_a into the rain attenuation can be expressed as follows

$$A = 10\log_{10}(T_a/(T_a-T_b)) \quad (4)$$

where A is the attenuation in unit of dB, T_b is the observed sky temperature in unit of K, T_a is the apparent rain temperature and the value of 273 K is used in converting T_b into A in this study, as suggested by Hogg and Chu (1975). Investigation shows that T_b increases with the increase of rainfall rate (Hogg, 1989), implying a positive correlation between A and rainfall rate. Figure 5 shows the one-minute resolution time series of rainfall rate recorded by optical rain gauge (middle panel) and the corresponding sky noise temperature observed by the radiometer (upper panel) which is pointed obliquely northeast at the elevation angle of 30°. It is obvious that a positive correlation between these two series is seen, irrespective of a time lag of 60 sec (lower panel) between them. After shifting the time axis to compensate the time lag and replotting the scatter diagram of rainfall rate versus sky noise temperature as presented in Figure 6, we can obtain an empirical expression relating the rainfall rate R to the sky noise temperature T_b as below

$$T_b = 102.4 + 8.044R \quad (5)$$

where the assumption that the apparent rain temperature is 275 K is made. With the help of equations (4) and (5), the rain attenuation can be estimated from the observation of rainfall rate.

5. CONCLUDING REMARKS

The statistical analysis of the long-term rainfall rates at one-minute time resolution recorded by more than 70 tipping bucket rain gauges distributed over Taiwan island from 1988 to 1995 is carried out in this article. It shows that a salient latitudinal variation of the rainfall rate intensity is found, greater in the southern part and weaker in the northern part of Taiwan. Using the 19.5 GHz microwave radiometer and high performance optical rain gauge imple-

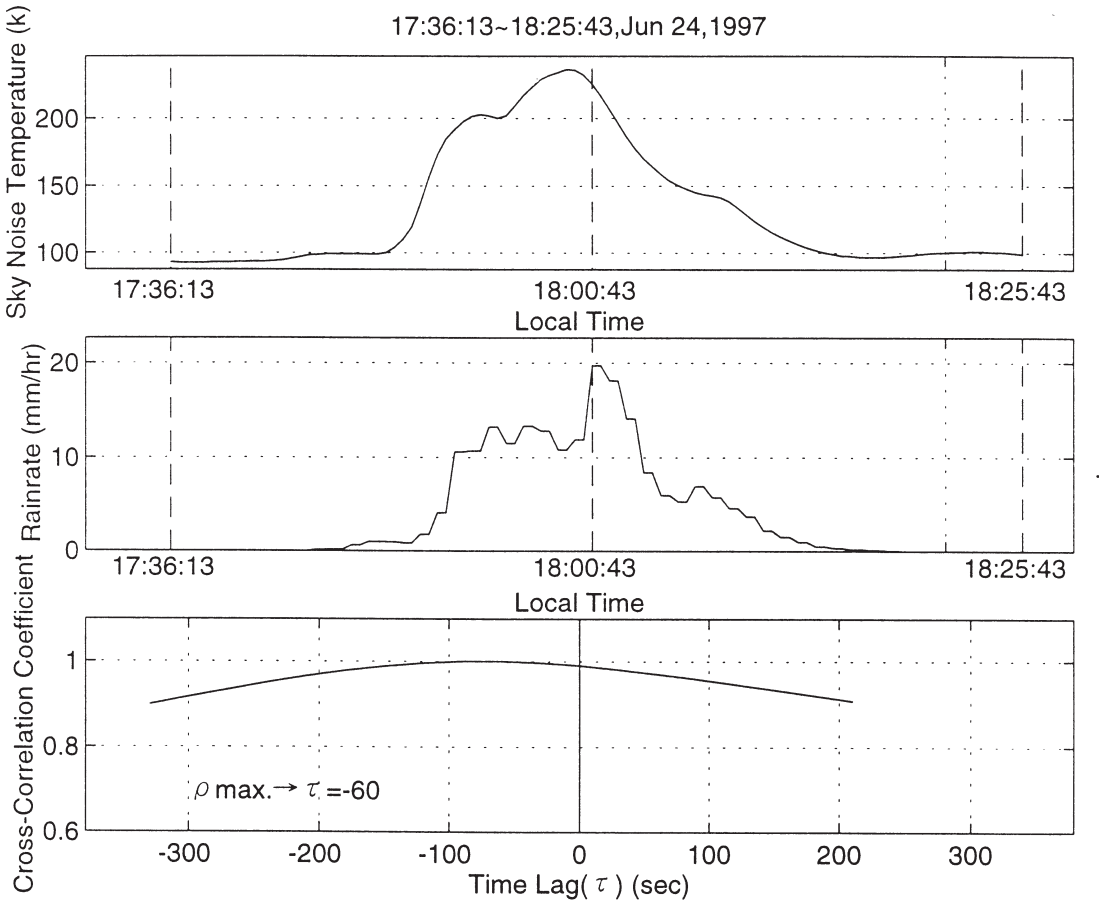

Fig. 5. Time series of rainfall rate at one-minute resolution recorded by optical rain gauge (middle panel) and the corresponding sky noise temperature observed by the radiometer (upper panel) which is pointed obliquely toward the northeast at the elevation angle of 30°. The cross correlation function between them is presented in the lower panel.

mented on the campus of National Central University at Chung-Li, we measure the clear-air sky noise temperature at different elevation angles. The results show that the clear-air sky noise temperature varies from 38 K at the elevation angle of 90° to 138 K at 15°, in perfect agreement with our theoretical calculation. The relation between the surface rainfall rate and the sky noise temperature from the rain drop is also analyzed and a regression line is obtained.

Acknowledgments This work was supported by the National Space Program Office (NSPO) of the Republic of China under the grants NSC86-NSPO-ECP-A-008-01, NSC86-NSPO-ECP-A-008-01, and NSC87-NSPO-ECP-A-008-01.

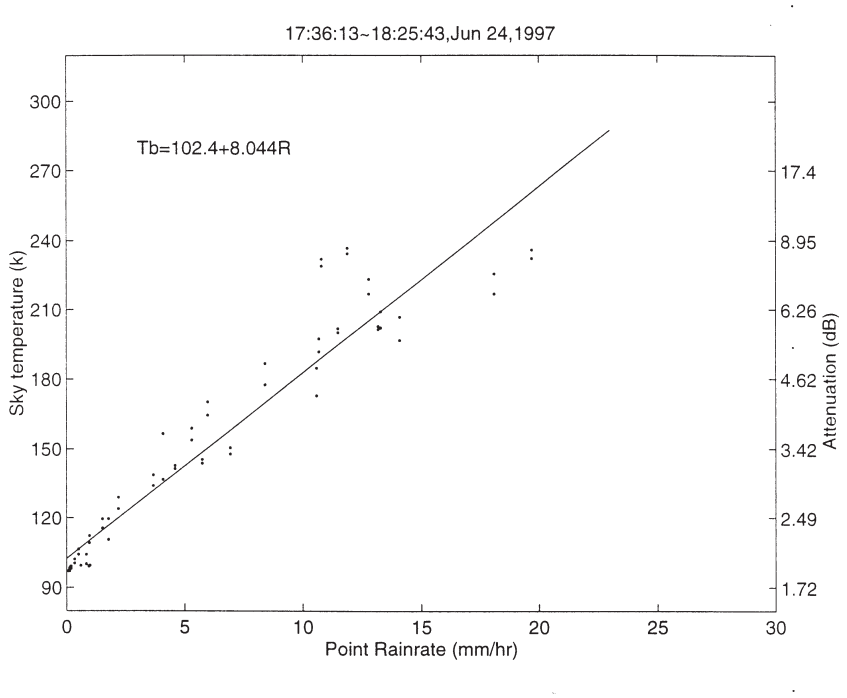

Fig. 6. Scatter diagram of rainfall rate versus sky noise temperature, in which the time lag between them is compensated as shown in figure 5.

REFERENCES

Chu, Y. H., L. P.Chian and C. H. Liu, 1991: The investigation of atmospheric precipitations by using Chung-Li VHF radar. *Radio Sci.*, **26**, 717-729.

Chu, Y. H. and C. H. Lin, 1994: The severe depletion of turbulent echo power in association of precipitation by using Chung-Li VHF radar. *Radio Sci* , 1311-1320.

Chu, Y. H. and J. S. Song, 1998: A combined observations of precipitation using Chung-Li VHF radar and ground-based optical rain gauge. *J. Geophys. Res.*, **103**, 11401-11409.

Crane, R. K., 1980: Prediction of Attenuation by Rain. Proc. IEEE Trans. Comm., **COM-28**, 1717.

Harrold, T. W., 1967: Attenuation of 8.6 mm Wavelength Radiation in Rain. *Proc. Inst. Elec. Eng.*, **114**, 201.

Hogg, D. C., Rain, 1989: Radiometry, and Radar. *IEEE Trans. Geosci. Remote Sensing*, **27**, 576.

Hogg, D. C. and T. S.Chu, 1975: The Role of Rain in Satellite Communications. *Proc. IEEE*, **63**, 1308.

Ippolito, Jr., L. J., Radiowave Propagation in Satellite Communication, Van Nostrand Reinhold

Compay, New York, NY (1986)

Ippolito, Jr., L.J. and T.A.Russell, 1993: Propagation Considerations for Emerging Satellite Communications Applications. *Proc. IEEE*, **81**, 923.

Olsen, R. L., D. V. Rogers and D. B.Hodge, 1978: The aR^b Relation in the Calculation of Rain Attenuation, IEEE Trans. Antenna Propagator., **AP-26**, 318.

Rottger, J., C. H. Liu, J. K. Chao, A. J. Chen, Y. H. Chu, I. J. Fu, C. M. Huang, Y. W. Kiang, F. S. Kuo, C. H. Lin and C. J. Pan, 1990: The Chung-Li VHF radar: Technical layout and a summary of initial results. *Radio Sci.*, **25**, 487-502.

Rogers, D. V., 1980: Propagation Analysis Package (PAP-2) Users Guide, COMSAT Labs. Tech. Mem. CL-9-80, January, sec.1.2.2.

Samplak, R. A. and R. H. Turrin, 1969: Some Measurements of Attenuation by Rainfall at 18.5 GHz. *Bell Syst. Tech. J.*, **48**, 1767.

Wakasugi, A. Mizutani and M. Matzuno, 1986: A direct method for deriving drop-size distribution and vertical air velocities from VHF Doppler radar spectra. *J. Atmos. Oceanic Technol.*, **3**, 623-629.